# Microwave sol-gel synthesis, microstructural and spectroscopic properties of scheelite-type ternary molybdate upconversion phosphor NaPbLa(MoO$_4$)$_3$:Er$^{3+}$/Yb$^{3+}$

Chang Sung Lim [a], Aleksandr S. Aleksandrovsky [b, c], Victor V. Atuchin [d, e, f, *], Maxim S. Molokeev [g, h, i], Aleksandr S. Oreshonkov [h, j]

[a] Department of Aerospace Advanced Materials & Chemical Engineering, Hanseo University, Seosan, 356-706, Republic of Korea
[b] Laboratory of Coherent Optics, Kirensky Institute of Physics Federal Research Center KSC SB RAS, Krasnoyarsk, 660036, Russia
[c] Department of Photonics and Laser Technologies, Siberian Federal University, Krasnoyarsk, 660041, Russia
[d] Laboratory of Optical Materials and Structures, Institute of Semiconductor Physics, SB RAS, Novosibirsk, 630090, Russia
[e] Functional Electronics Laboratory, Tomsk State University, Tomsk, 634050, Russia
[f] Research and Development Department, Kemerovo State University, Kemerovo, 650000, Russia
[g] Laboratory of Crystal Physics, Kirensky Institute of Physics, Federal Research Center KSC SB RAS, Krasnoyarsk, 660036, Russia
[h] Siberian Federal University, Krasnoyarsk, 660041, Russia
[i] Department of Physics, Far Eastern State Transport University, Khabarovsk, 680021, Russia
[j] Laboratory of Molecular Spectroscopy, Kirensky Institute of Physics Federal Research Center KSC SB RAS, Krasnoyarsk, 660036, Russia

## ARTICLE INFO

## ABSTRACT

New ternary molybdate NaPbLa$_{(1-x-y)}$(MoO$_4$)$_3$:$x$Er$^{3+}$,$y$Yb$^{3+}$ ($x = y = 0$, $x = 0.05$ and $y = 0.35$, 0.4, 0.45 and 0.5) phosphors were successfully fabricated by the MSG (microwave sol-gel) method, and the microstructural and spectroscopic properties were characterized. The crystal structure of NaPbLa(MoO$_4$)$_3$ (NPLM) was defined by Rietveld analysis in space group $I4_1/a$ with unit cell parameters $a = 5.3735(2)$ and $c = 11.8668(4)$ Å, $V = 342.65(3)$ Å$^3$, $Z = 4$ ($R_B = 6.64\%$). The unit cell volume of NaPbLa(MoO$_4$)$_3$ (NPLM) was intermediate between those of NaLa(MoO$_4$)$_2$ and PbMoO$_4$. Under the 980 nm excitation, upconverted yellowish-green emissions at transitions from $^2$H$_{11/2}$ and $^4$S$_{3/2}$ were observed. No concentration quenching in the subsystem of donor ions at the content up to 50 at.% and no cross-relaxation losses in the subsystem of acceptor ions at the concentrations as high as 5 at. % were verified. The individual chromaticity points for the NaPbLa(MoO$_4$)$_3$:Er$^{3+}$,Yb$^{3+}$ phosphors, corresponding to the equal-energy point in the standard CIE diagram, revealed yellowish-green emissions.

© 2019 Published by Elsevier B.V.

## 1. Introduction

For the recent years, complex molybdate crystals have become of extensive interest due to their stable chemical properties, rich crystal chemistry and potential applications in such fields as laser systems, electrochemistry and photonics [1–10]. Complex molybdates are actively investigated as host materials for the creation of rare-earth doped phosphors appropriate for the use in light-emitting devices [1,2,11–15]. Among such crystals, scheelite-type molybdates are widely investigated in terms of searching new structures, including structure-modulation effects, and promising spectroscopic characteristics [15–19]. One of the most representative scheelite-type molybdates is the PbMoO$_4$ compound, which is suitable for laser application, can be used as a low temperature scintillator crystal and as a working medium in an acoustic-optical light modulator [20–22]. In view of the above mentioned properties, it is interesting to investigate the effects of Pb ion combined with other cations in the scheelite framework. It is known that, in simple molybdates, the scheelite-type structure is comparatively stable and a wide size range of big A$^{2+}$ (A = Cd–Ba) cations can be accommodated without structure disruptions [23–25]. However, in binary molybdates, the cation combinations, appropriate for a scheelite-type structure, are less clear and only tentative predictions are possible depending on the average big cation size [16,26,27]. In ternary molybdates, the rules governing the scheelite structure stability are unclear.

Recently, a new family of ternary molybdates of the scheelite-type structure has been discovered and efficient upconversion (UC) phosphors have been prepared on the base of these hosts [28,29]. The present study is aimed at the preparation and evaluation of new ternary molybdate $NaPbLa(MoO_4)_3$ (NPLM), where a bigger-sized $Pb^{2+}$ cation is introduced instead of $Ca^{2+}$ and $Sr^{2+}$ in $NaALa(MoO_4)_3$ (A = Ca, Sr) [30]. The substitution results in the bigger average ion radius of cation complex (NaALa) and related structural and spectroscopic effects, respectively, can be considered. Additionally, the NPLM:$Er^{3+}$,$Yb^{3+}$ phosphors will be prepared to estimate the potential of the NPLM host in optical frequency UC structures.

Among rare-earth ions, the $Er^{3+}$ ion is suitable for the optical frequency conversion via the UC process due to its appropriate configuration of electronic energy levels. The $Yb^{3+}$ ion, commonly used as a sensitizer, can be efficiently excited by an IR light source functional at ~980 nm. Then, the absorbed energy is transferred to the activator ions ($Er^{3+}$) and that drastically increases the emission efficiency. Thus, the $Er^{3+}$/$Yb^{3+}$ co-doping can remarkably enhance the UC efficiency for the shift from infrared to visible light due to the efficiency of the energy transfer from $Yb^{3+}$ to $Er^{3+}$ [31–35]. In the present study, the pure and doped ternary molybdate $NaPbLa_{(1-x-y)}(MoO_4)_3$:$xEr^{3+}$,$yYb^{3+}$ (NPLM:$xEr^{3+}$,$yYb^{3+}$) powder samples with the correct doping concentrations of $Er^{3+}$ and $Yb^{3+}$ ($x = y = 0$, $x = 0.05$ and $y = 0.35$, 0.4, 0.45 and 0.5) were successfully synthesized by the MSG (microwave sol-gel) method followed by a high-temperature treatment in the air. As it was shown earlier, this method is highly efficient for the preparation of complex molybdate and tungstate compounds for a relatively short time [36–39]. The prepared powder samples were characterized by the X-ray diffraction (XRD) for Rietveld refinement and scanning electron microscopy (SEM). The Raman and photoluminescence (PL) emission spectra were examined comparatively for different doping levels. The dependence of pump power and Commission Internationale de L'Eclairage (CIE) chromaticity parameters of the UC emission were evaluated in detail.

## 2. Experimental

In the present experiment, $Na_2MoO_4 \cdot 2H_2O$, $Pb(NO_3)_2$, $La(NO_3)_3 \cdot 6H_2O$ and $(NH_4)_6Mo_7O_{24} \cdot 4H_2O$ at the purity of 99.0%, and $Yb(NO_3)_3 \cdot 5H_2O$, and $Er(NO_3)_3 \cdot 5H_2O$ at the purity of 99.9% were used as received from Sigma-Aldrich, USA. Besides, citric acid at the purity of 99.5% was received from Daejung Chemicals, Korea. Distilled water, ethylene glycol (A.R.) and $NH_4OH$ (A.R.) were used to bring the transparent sol formation. As the first step, to prepare the sol of (a) $NaPbLa(MoO_4)_3$ (NPLM), $Na_2MoO_4 \cdot 2H_2O$ for 0.2 mol% and $(NH_4)_6Mo_7O_{24} \cdot 4H_2O$ for 0.143 mol% were dissolved in 80 mL 8 M $NH_4OH$ with 20 mL ethylene glycol. Subsequently, $Pb(NO_3)_3$ for 0.4 mol% and $La(NO_3)_3 \cdot 5H_2O$ for 0.4 mol% were precisely weighed and dissolved slowly in 100 mL distilled water. Then, the two solutions were mixed together under vigorous stirring and the mixture was adjusted to $pH = 7-8$ using citric acid and $NH_4OH$. At this stage, a citric acid molar ratio accounting for the numbers of total cation metal ions is adjusted to 2:1. The appropriate amount of the solution, 180–200 mL, was heated up to 80–100 °C in a 450 mL Pyrex glass before the MSG processing. Consequently, the final solution becomes highly transparent.

As for the doped compounds of $NaPbLa_{(1-x-y)}(MoO_4)_3$:$xEr^{3+}$,$yYb^{3+}$ (NPL$_{(1-x-y)}$M:$xEr^{3+}$$yYb^{3+}$), the following variations were made to prepare the solutions for: (b) NPLa$_{0.6}$M:$Er_{0.05}Yb_{0.35}$, $La(NO_3)_3 \cdot 6H_2O$ for 0.24 mol%, $Yb(NO_3)_3 \cdot 5H_2O$ for 0.14 mol% and $Er(NO_3)_3 \cdot 5H_2O$ for 0.02 mol%; (c) NPLa$_{0.55}$M:$Er_{0.05}Yb_{0.4}$, $La(NO_3)_3 \cdot 6H_2O$ for 0.22 mol%, $Yb(NO_3)_3 \cdot 5H_2O$ for 0.16 mol% and $Er(NO_3)_3 \cdot 5H_2O$ for 0.02 mol%; (d) NPLa$_{0.5}$M:$Er_{0.05}Yb_{0.45}$, $La(NO_3)_3 \cdot 6H_2O$ for 0.2 mol%, $Yb(NO_3)_3 \cdot 5H_2O$
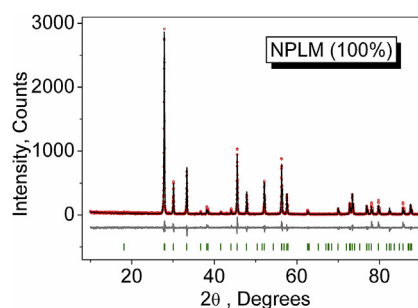


**Fig. 1.** The difference Rietveld plot of NPLM.

for 0.18 mol% and $Er(NO_3)_3 \cdot 5H_2O$ for 0.02 mol%; and (e) NPLa$_{0.45}$M:$Er_{0.05}Yb_{0.5}$, $La(NO_3)_3 \cdot 6H_2O$ for 0.18 mol%, $Yb(NO_3)_3 \cdot 5H_2O$ for 0.2 mol% and $Er(NO_3)_3 \cdot 5H_2O$ for 0.02 mol%.

For the MSG process, a useful microwave oven was utilized at the frequency of 2.45 GHz and the maximum output power with 1250 W for 30 min. The mixed solutions were located in the oven under two kinds of cyclic working steps. At the first step, the MSG process was controlled by the cyclic regime of 40 s on and 20 s off for 15 min. At the second step, the further treatment was continued by the cyclic regime of 30 s on and 30 s off for 15 min. After the MSG process, the sols were treated under ultrasonic radiation for 10 min to obtain light yellow colored transparent sols. The transparent sols were dried at 120 °C in a dry oven for one week. The obtained black dried gels were ground, heat treated at 350 °C for 6 h to evaporate ethylene glycol and other remained organic substances and annealed at 850 °C for 16 h. As it was previously stated, this temperature range is highly appropriate for the calcination of molybdate compounds [3,6,40–42]. After the annealing process, pink colored particles were obtained for the doped samples.

The powder diffraction patterns of the new ternary molybdate NPLM: $Er^{3+}$,$Yb^{3+}$ particles for Rietveld analysis were precisely examined over the range of $2\theta = 5-90°$ at room temperature with a D/MAX 2200 (Rigaku in Japan) diffractometer with the Cu-K$\alpha$ radiation and $\theta$-$2\theta$ geometry. The size step of $2\theta$ was 0.02°, and the time counting was 5 s per step. The TOPAS 4.2 package was applied for the Rietveld analysis [43]. The typical microstructure and surface morphology of the obtained particles were observed using SEM (JSM-5600, JEOL in Japan). The synthesized powder samples were prepared on a copper cylinder with diameters of 8 mm. The sample surface was coated by the Au coating using a sputtering equipment to avoid surface charging effects, sample decomposition, chemical reactions, morphology deformations, phase and contrast transformations by a charge-up of the electron beam. The coating thickness were controlled to be in the range of 50–200 Å. The PL spectra were relatively recorded using a spectrophotometer (PerkinElmer LS55 in UK) at room temperature. The pump power dependence of the resultant UC emission intensity was measured at the working power from 20 to 110 mW levels. The Raman spectra measurements were performed using a LabRam Aramis (Horiba Jobin-Yvon in France) with the spectral resolution of 2 $cm^{-1}$. The synthesized powder samples were prepared randomly on a clean slide glass. The 514.5-nm line of an Ar ion laser was used as an excitation source; the power on the samples was kept at the 0.5 mW level to avoid the sample decomposition. The doped samples were compared with the undoped sample in the spectral region of 100–1400 $cm^{-1}$.

## 3. Results and discussion

The XRD pattern measured for NPLM is shown in Fig. 1 and the patterns of doped samples are shown in Figs. S1–S4 (Supporting

Information). All peaks of the powder patterns recorded from NaPbLa$_{1-x-y}$MoO$_4$: $x$Er$^{3+}$,$y$Yb$^{3+}$ ($x = 0$, 0.05; $y = 0$, 0.35, 0.4, 0.45, 0.5) compounds were successfully indexed by the tetragonal cell ($I4_1/a$) with cell parameters close to those of PbMoO$_4$ [44]. Therefore, the crystal structure of PbMoO$_4$ was taken as a starting model for Rietveld refinement. The Pb$^{2+}$ ion site was considered as occupied by Pb, Na, La, Er, Yb ions (Fig. 2) with fixed occupations according to the suggested formulas. The refinements were stable and gave low R-factors (Table 1, Fig. 1, S1−S4). The coordinates of atoms and the main bond lengths are summarized in Tables S1 and S2, respectively.

Further details of the crystal structures may be obtained from Fachinformationszentrum Karlsruhe, 76344 Eggenstein-Leopoldshafen, Germany (fax: (+49)7247-808-666; E-mail: crystdata@fiz-karlsruhe.de; http://www.fiz-karlsruhe.de/request_for_deposited_data.html on quoting the deposition numbers: CSD-1898247; CSD-18982248; CSD-1898249; CSD-1898250; CSD-1898251.

The cell volume dependence on the average ion radius of big cations IR(Na/Pb/La/Er//Yb), excluding Mo$^{6+}$, in the NPLM:Er$^{3+}$,Yb$^{3+}$ compounds is shown in Fig. 3a. The diagram part containing ternary molybdates can be observed in Fig. S5. The IR values were calculated on the base of nominal compositions and the known system of ion radii [30]. It is evident that the cell volume linearly decreases with the IR(Na/Pb/La/Er//Yb) decrease or the ($x + y$) increase. This clearly proves the suggested chemical formulas of solid solutions NPLM:Er$^{3+}$,Yb$^{3+}$. Besides, it is very interesting to see the position of NPLM:Er$^{3+}$,Yb$^{3+}$ compounds among other known scheelite-type molybdates. In Fig. 3b, the cell volume of selected simple and complex scheelite-type molybdates is shown as a function of big cation ion radius (IR), where, for the complex compounds, the average ion radius of big cations is calculated on the base of available information [24,28−30,44−50]. Accounting the big cation valencies in NaPbLa(MoO$_4$)$_3$ and mixed occupancy of unique cation position, the formula can be written as (Na$_{1/3}$Pb$_{1/3}$La$_{1/3}$)$^{2+}$MoO$_4$. On this basis, the structure relation can be considered between NaPbLa(MoO$_4$)$_3$ and A$^{2+}$MoO$_4$ (A = Cd, Ca, Eu, Sr, Ba) molybdates. To develop the available data set, the crystal structures of the NaCaGd(MoO$_4$)$_3$:Er$^{3+}$/Yb$^{3+}$ compounds were defined by Rietveld method with the use of the experimental results obtained in Ref. 50. Further details of the crystal structures may be obtained from Fachinformationszentrum Karlsruhe, 76344 Eggenstein-Leopoldshafen, Germany (fax: (+49)7247-808-666; E-mail: crystdata@fiz-karlsruhe.de; http://www.fiz-karlsruhe.de/request_for_deposited_data.html on quoting the deposition numbers: CSD-1898252; CSD-18982253; CSD-1898254; CSD-1898255.

The basic curve is generated by simple molybdates with general composition A$^{2+}$MoO$_4$ (A = Cd, Ca, Eu, Sr, Ba) and the drastic unit cell variation 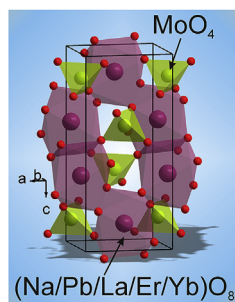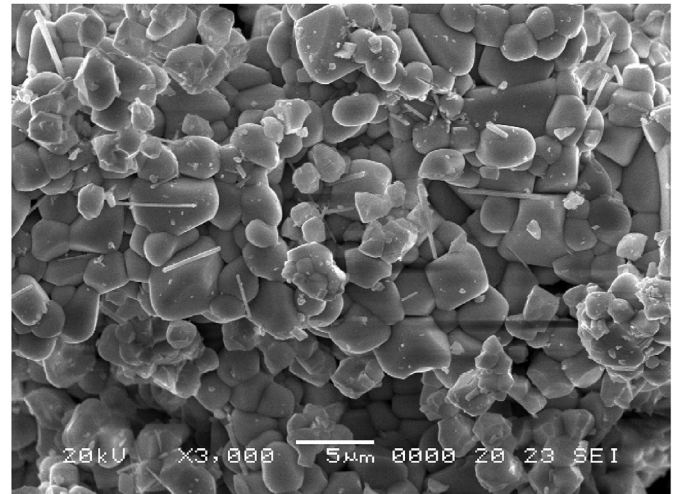by 25% is evident on the A$^{2+}$ cation substitutions. This indicates an extremely high stability of the scheelite-type structure in reference to the element substitution at the A$^{2+}$ position. The point of binary scheelite NaLa(MoO$_4$)$_2$ is not very far from the main line and its structural properties should be governed by the general tendency. Indeed, the addition of the [CaMoO$_4$] block to the composition NaLa(MoO$_4$)$_2$ results in the formation of scheelite-type compound NaCaLa(MoO$_4$)$_3$, which cell volume is intermediate between those of NaLa(MoO$_4$)$_2$ and CaMoO$_4$. The similar trend is observed when the [PbMoO$_4$] block is added to the composition NaLa(MoO$_4$)$_2$ with the formation of NPLM, which unit cell volume is intermediate between those of NaLa(MoO$_4$)$_2$ and PbMoO$_4$. According to this algorithm, the existence of a wide family of scheelite-type compounds NaA$^{2+}$La(MoO$_4$)$_3$ can be predicted. Within possible cation combinations, the substitution of the [BaMoO$_4$] block to NaLa(MoO$_4$)$_2$ is of special interest because, in this case, the particularly big variation of the unit cell volume can be assumed in reference to that of NaLa(MoO$_4$)$_2$. Above this, the existence of NaA$^{2+}$Ln(MoO$_4$)$_3$ (Ln = rare earth elements) compounds is also supposed and it is promising for the use of NaA$^{2+}$Ln(MoO$_4$)$_3$ hosts in photonics because a wide range rare earth element substitution is possible at the Ln position without a structure destruction and drastic defect generation.

The SEM images obtained for the representative compositions (a) NPLM and (b) NPLM:0.05Er$^{3+}$,0.5 Yb$^{3+}$ are shown in Fig. 4. Both samples contain closely packed grains sized 10−25 μm. The grain micromorphology in both samples is very similar. This means that the rare-earth ion substitution at the La$^{3+}$ sites in NPLM has no influence on the micromorphology.
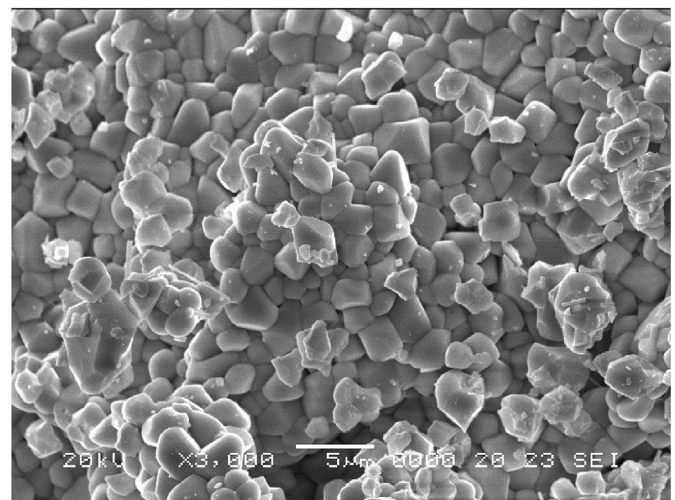
The Raman spectrum of the synthesized NPLM is shown in Fig. 5. It can be divided into three spectral regions: 950−700, 425−275 and 275−100 cm$^{-1}$. The observed bands consist of internal vibrations of MoO$_4^{2-}$ ions and external vibrations [51]. The isolated MoO$_4$ tetrahedron has four normal vibrational modes: $\nu_1(A_1)$, $\nu_2(E)$, $\nu_3(F_2)$ and $\nu_4(F_2)$, where letters $A$, $E$, and $F$ refer to nondegenerate, double and triple degenerate vibrations, correspondingly [52]. These modes correspond to the following vibrations: $\nu_1$ − symmetric stretching, $\nu_2$ − symmetric bending, $\nu_3$ − asymmetric stretching and $\nu_4$ − asymmetric bending. All four vibrational modes are Raman-active. The MoO$_4^{2-}$ ions in NPLM ($C_{4h}$ factor group symmetry) occupy the sites ($S_4$) of lower symmetry than "free" MoO$_4^{2-}$ ions ($T_d$) and that leads to removing the degeneracies of normal modes: $A_1 \rightarrow A_g + B_u$, $E \rightarrow A_g + B_u + B_g + A_u$, $F_2 \rightarrow B_g + A_u + E_g + E_u$. The rotation and translational vibrations under the $T_d$ symmetry transform as $F_1 \rightarrow A_g + B_u + E_g + E_u$ and $F_2 \rightarrow B_g + A_u + E_g + E_u$ correspondingly. The vibrational representation for the tetragonal unit cell of NPLM at the Brillouin zone center is given by the following equation: $\Gamma_{vibr} = 3A_g + 7A_u + 7B_g + 3B_u + 14E_g + 14E_u$. According to the selection rules, the $A_g$, $B_g$ and $E_g$ modes are Raman active, $A_u$ and $E_u$ are IR active, and $B_u$ modes are silent. Thus, three Raman bands should be observed in the region of stretching vibrations and four bands - in the region of the bending vibrations of MoO$_4$ tetrahedra. The strong Raman band at 881.2 cm$^{-1}$ ($A_g$) is assigned to the $\nu_1$ vibrational mode of the MoO$_4^{2-}$ ion, and the bands at 818.6 ($B_g$) and 757.3 cm$^{-1}$ ($E_g$) are assigned to the $\nu_3$ modes. The $\nu_4$ asymmetric vibrations appear at 380.1 ($B_g$) and 366.9 cm$^{-1}$ ($E_g$), and the bands at 326.4 ($B_g$) and 319.0 cm$^{-1}$ ($A_g$) are the $\nu_2$ vibrational modes. The deconvolution of experimental Raman spectrum by fitting with the use of Lorentzian function revealed extra bands at 900.4, 795.1, 668.3 and 292.6 cm$^{-1}$. The appearance of these lines can be explained as the local distortions of MoO$_4$ tetrahedra caused by the influence of Na/Pb/La ions. The wide band at 230.6 cm$^{-1}$ is assigned to the rotation of MoO$_4^{2-}$ ions. The other bands in the low-wavenumber region of the Raman spectrum are external modes (translations of MoO$_4^{2-}$ and Na/Pb/La ions and their mixed vibrations).



**Fig. 2.** The crystal structure of NPLM. The unit cell is outlined. The lone atoms are omitted for clarity.

**Table 1**
Main parameters of processing and refinement of the NPLM:$x$Er$^{3+}$,$y$Yb$^{3+}$ samples.

| Compound | Space group, Z | Cell parameters (Å), cell volume (Å$^3$) | $R_p$ (%), R$_{wp}$ (%), $R_B$ (%), $\chi^2$ |
|---|---|---|---|
| NPLM | $I4_1/a$, 4 | $a = 5.3735$ (2) $c = 11.8668$ (4) $V = 342.65$ (3) | 14.16, 19.90, 6.64 1.30 |
| NPLM: 0.05Er,0.35 Yb | $I4_1/a$, 4 | $a = 5.3301$ (4) $c = 11.756$ (1) $V = 333.99$ (6) | 13.14, 18.54, 4.52 1.31 |
| NPLM: 0.05Er,0.4 Yb | $I4_1/a$, 4 | $a = 5.3208$ (2) $c = 11.7284$ (5) $V = 332.04$ (3) | 12.95, 18.09, 4.85 1.35 |
| NPLM: 0.05Er,0.45 Yb | $I4_1/a$, 4 | $a = 5.3150$ (2) $c = 11.7189$ (7) $V = 331.06$ (4) | 11.66, 16.44, 2.63 1.23 |
| NPLM: 0.05Er,0.5 Yb | $I4_1/a$, 4 | $a = 5.3099$ (2) $c = 11.7010$ (5) $V = 329.91$ (2) | 10.91, 15.74, 2.49 1.11 |

In case of the NPLM doped with Er$^{3+}$ and Yb$^{3+}$ ions, the Raman spectra are totally covered with the luminescence signal of Er$^{3+}$ ions, as shown in Fig. 6. Only the very small peak at 881.2 cm$^{-1}$ related to symmetric stretching vibration of MoO$_4$ tetrahedra can be distinguished in the spectra. It should be noted that an increase of the Yb$^{3+}$ content leads to the difference of Er$^{3+}$ $^2$H$_{11/2}$ multiplet intensity. This fact can be explained in the framework of the different local structure of Er$^{3+}$, as induced by the Yb$^{3+}$ doping level variation (Table S2).

The UC luminescence spectra of NPLM coactivated by 5% of Er$^{3+}$ ions and the increasing content of Yb$^{3+}$ ions measured at room temperature under the 980 nm excitation are presented in Fig. 7. The UC emission in green color region at the transition from the $^4$H$_{11/2}$ state to the $^4$I$_{15/2}$ ground state is prevailing over the emission at the transition from $^4$S$_{3/2}$ to $^4$H$_{15/2}$, while the deep red emission at



**(a)**



**(b)**

**Fig. 4.** Scanning electron microscopy images of the synthesized (a) NPLM and (b) NPLM:0.05Er$^{3+}$,0.5 Yb$^{3+}$ particles.



a



b
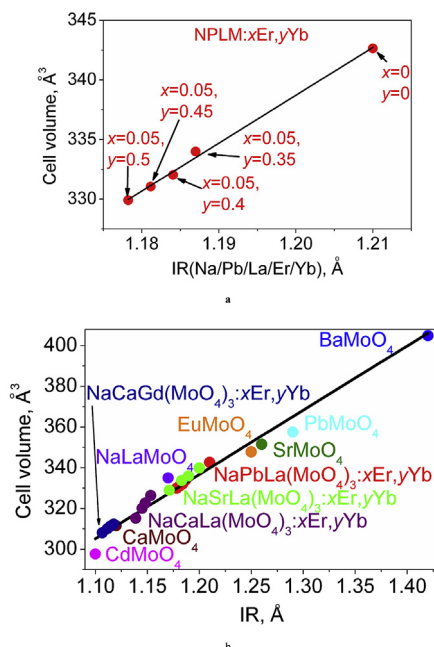
**Fig. 3.** (a) The dependence of cell volume on averaged ion radii IR(Na/Pb/La/Er/Yb) of NPLM: $x$Er$^{3+}$,$y$Yb$^{3+}$ and (b) the NPLM: $x$Er$^{3+}$,$y$Yb$^{3+}$ crystals among other representative scheelite-type molybdates.

the transition from $^4$F$_{9/2}$ to $^4$H$_{15/2}$ is approximately 25 times weaker in all samples, as compared to the green emission. The increase of the Yb$^{3+}$ content from 35 to 50% results in a continuous growth of the UC emission at all lines indicating the absence of concentration quenching in the subsystem of Yb ions up to the doping level as high as 50%. The power dependences of UCL (Fig. 8) show slopes with n < 2 and that indicates the absence of the cross-relaxation in the system of Er$^{3+}$ ions at the concentration as high as 5%. For the most prominent example of cross-relaxation influence on the UC behavior at 5% Er in CsScF$_4$ host, see Ref. [53]. The features specified above must be ascribed to the advantages of the used molybdate crystalline matrix.

The CIE diagram and chromaticity coordinates ($x$, $y$) of NPLM:Er$^{3+}$,Yb$^{3+}$ phosphors are shown in Fig. 9 The individual CIE chromaticity points for samples (a), (b), (c) and (d) are exhibited by the legend in Fig. 8A. The calculated values for chromaticity coordinates are $x = 0.237$ and $y = 0.669$ for (a), $x = 0.246$ and
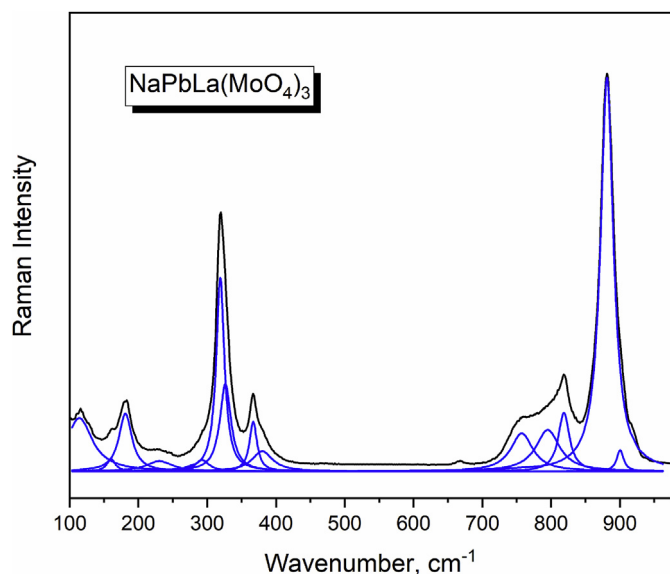
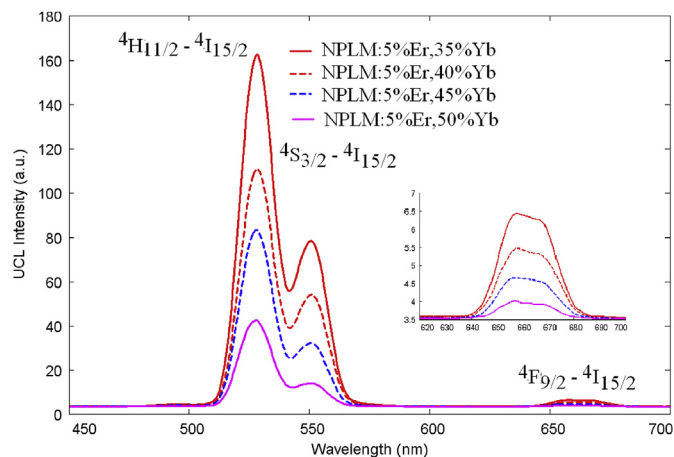**Fig. 5.** Raman spectrum of NPLM powder. The fitting was done using the Lorentzian function.
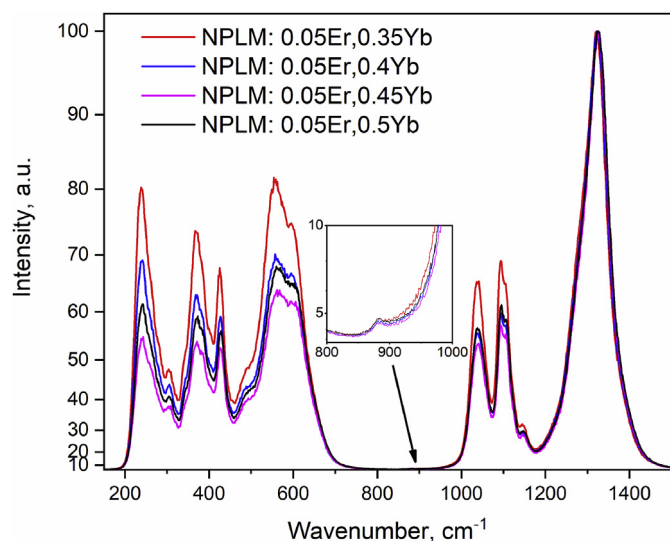


**Fig. 6.** The luminescence from $^2H_{11/2}$ and $^4S_{3/2}$ multiples of the $Er^{3+}$ ions normalized to the most intense band of $^4S_{2/3}$ multiplet in the region of the lattice vibrations of NPLM: $xEr^{3+}, yYb^{3+}$.



**Fig. 7.** The UC photoluminescence spectra of (a) $NPLM:0.05Er^{3+},0.35\,Yb^{3+}$, (b) $NPLM:0.05Er^{3+},0.40\,Yb^{3+}$, (c) $NPLM:0.05Er^{3+},0.45\,Yb^{3+}$, and (d) $NPLM:0.05Er^{3+},0.50\,Yb^{3+}$ particles excited under 980 nm at room temperature.



**Fig. 8.** The UC emission intensity logarithmic scale dependence on the pump power in the range from 20 to 110 mW at 525, 550 and 655 nm in the $NPLM:0.05Er^{3+},0.35\,Yb^{3+}$ sample.
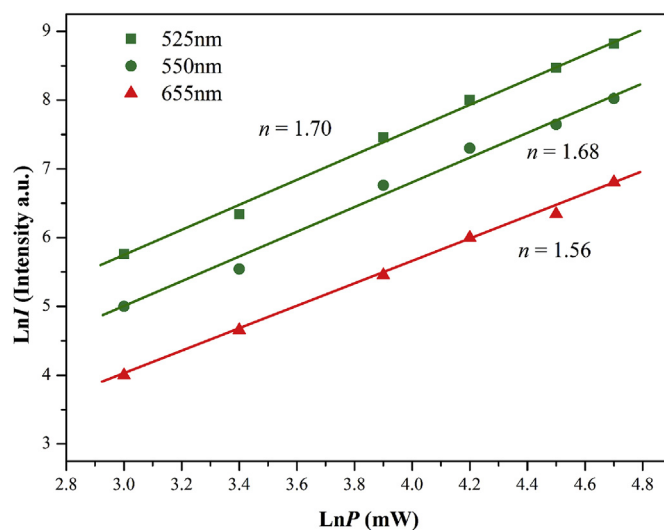
$y = 0.640$ for (b), $x = 0.248$ and $y = 0.610$ for (c), and $x = 0.269$, and $y = 0.529$ for (d), corresponding to the equal-energy point in the standard CIE diagram. As it is seen, the $NaPbLa(MoO_4)_3:Er^{3+},Yb^{3+}$ phosphors provide the emission in the yellowish-green region.

## 4. Conclusions

New ternary molybdate $NPLM:Er^{3+},Yb^{3+}$ phosphors were successfully synthesized by the MSG method, and the microstructural and spectroscopic properties were investigated in detail. The general dependence of the unit cell on the average ion radii of all cations, excluding $Mo^{6+}$, in the scheelite type molybdates was defined with the use of available experimental data on the crystal structures. The NPLM unit cell volume was intermediate between those of $NaLa(MoO_4)_2$ and $PbMoO_4$. The diagram provides the predictions of the existence of a wide family of scheelite-type compounds $NaA^{2+}La(MoO_4)_3$ (A = Cd−Ba) with a great potential for the creation of new phosphor materials. The rare-earth ion substitution at the $La^{3+}$ sites in NPLM had no influence on the micromorphology variation. The Raman spectra of the NPLM doped with $Er^{3+}$ and $Yb^{3+}$ ions were totally covered with the luminescence signal of $Er^{3+}$ ions, and increasing the $Yb^{3+}$ content resulted in the difference of the $Er^{3+}$ $^2H_{11/2}$ multiplet intensity. The individual chromaticity points for the $NPLM:Er^{3+},Yb^{3+}$ phosphors corresponding to the equal-energy point in the standard CIE diagram indicated the yellowish-green emissions. The crystalline matrix under investigation favors the domination of the yellowish-green upconverted emission of $Er^{3+}$ ions and enables the absence of concentration quenching up to the Yb content as high as 50%, as well as the absence of cross-relaxation at the $Er^{3+}$ content as high as 5%. This phosphor can be employed for the solar radiation spectrum transformations in solar energetics.
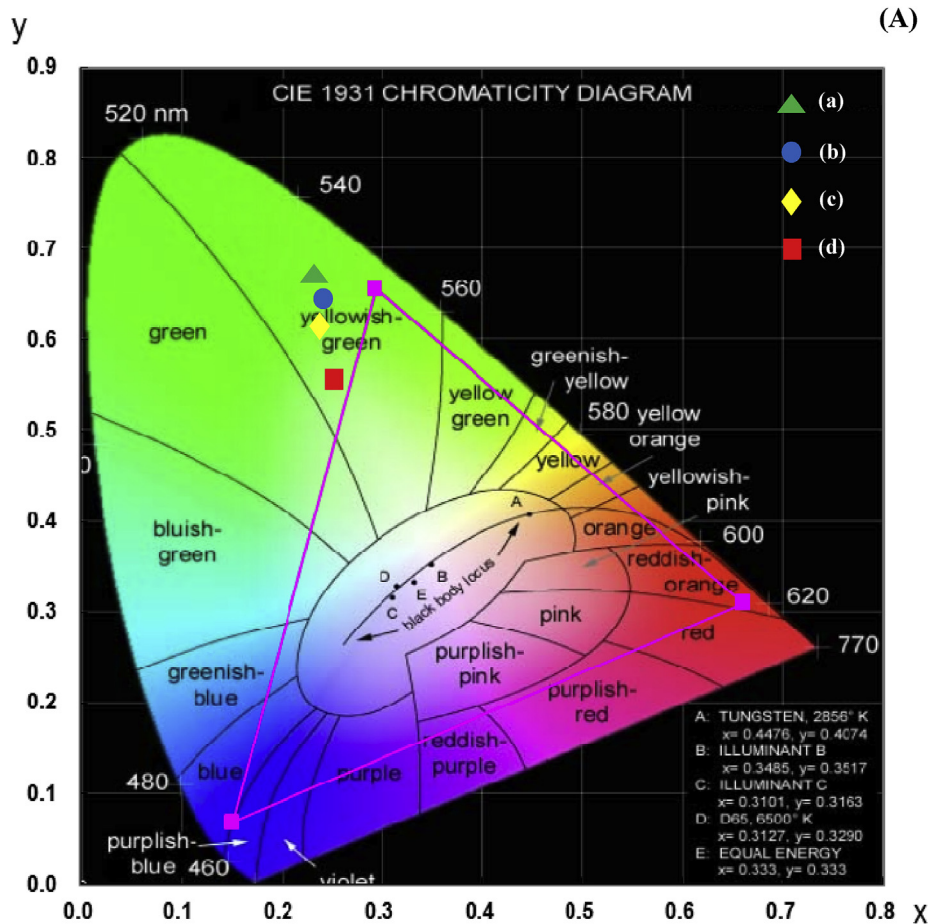
**Fig. 9.** (A) CIE chromaticity diagram for the NPLM:$x$Er$^{3+}$,$y$Yb$^{3+}$ phosphors, and (B) calculated chromaticity coordinate (x, y) values. The emission points for the sample (a) NPLM:0.05Er$^{3+}$,0.35 Yb$^{3+}$, (b) NPLM:0.05Er$^{3+}$,0.40 Yb$^{3+}$, (c) NPLM:0.05Er$^{3+}$,0.45 Yb$^{3+}$, and (d) NPLM:0.05Er$^{3+}$,0.50 Yb$^{3+}$ particles are shown in the legend.

## Appendix A. Supplementary data

Supplementary data to this article can be found online at https://doi.org/10.1016/j.jallcom.2019.152095.

## References

[1] Katrien W. Meert, Vladimir A. Morozov, Artem M. Abakumov, Joke Hadermann, Dirk Poelman, Philippe F. Smet, Energy transfer in Eu$^{3+}$ doped scheelites: use as thermographic phosphor, Opt. Express 22 (2014) A961−A972. https://doi.org/10.1364/OE.22.00A961.

[2] Pinglu Shi, Zhiguo Xia, Maxim S. Molokeev, Victor V. Atuchin, Crystal chemistry and luminescence properties of red-emitting $CsGd_{1-x}Eu_x(MoO_4)_2$ solid-solution phosphors, Dalton Trans. 43 (2014) 9669–9676. https://doi.org/10.1039/c4dt00339j.

[3] A.A. Savina, V.V. Atuchin, S.F. Solodovnikov, Z.A. Solodovnikova, A.S. Krylov, E.A. Maksimovsky, M.S. Molokeev, A.S. Oreshonkov, A.M. Pugachev, E.G. Khaikina, Synthesis, structural and spectroscopic properties of acentric triple molybdate $Cs_2NaBi(MoO_4)_3$, J. Solid State Chem. 225 (2015) 53–58. https://doi.org/10.1016/j.jssc.2014.11.023.

[4] Sergei Kurilchik, Pavel Loiko, Anatol Yasukevich, Vyacheslav Trifonov, Volokitina Anna, Vilejshikova Elena, Viktor Kisel, Xavier Mateos, Aleksander Baranov, Oleg Goriev, Nikolay Kuleshov, Anatoly Pavlyuk, Orthorombic $Yb:Li_2Zn_2(MoO_4)_3$ – a novel potential crystal for broadly tunable lasers, Laser Phys. Lett. 14 (2017), 085804. https://doi.org/10.1088/1612-202X/aa7603.

[5] Aleksandra A. Savina, Vladimir A. Morozov, Anton L. Buzlukov, Irina Yu Arapova, Sergey Yu Stefanovich, Yana V. Baklanova, Tatiana A. Denisova, Nadezhda I. Medvedeva, Michel Bardet, Joke Hadermann, Bogdan I. Lazoryak, Elena G. Khaikina, New solid electrolyte $Na_9Al(MoO_4)_6$: structure and Na+ ion conductivity, Chem. Mater. 29 (2017) 8901–8913. https://doi.org/10.1021/acs.chemmater.7b03989.

[6] Sergey F. Solodovnikov, Victor V. Atuchin, Zoya A. Solodovnikova, Oleg Y. Khyzhun, Mykola I. Danylenko, Denis P. Pishchur, Pavel E. Plyusnin, Alexey M. Pugachev, Tatiana A. Gavrilova, Alexander P. Yelisseyev, Ali H. Reshak, Zeyad A. Alahmed, Nadir F. Habubi, Synthesis, structural, thermal, and electronic properties of palmierite-related double molybdate $\alpha$-$Cs_2Pb(MoO_4)_2$, Inorg. Chem. 56 (6) (2017) 3276–3286. https://doi.org/10.1021/acs.inorgchem.6b02653.

[7] Shriya Sinha, Kaushal Kumar, Studies on up/down-conversion emission of $Yb^{3+}$ sensitized $Er^{3+}$ doped $MLa_2(MoO_4)_4$ (M = Ba, Sr and Ca) phosphors for thermometry and optical heating, Opt. Mater. 75 (2018) 770–780. https://doi.org/10.1016/j.optmat.2017.10.036.

[8] Pavel Loiko, Esrom Kifle, Josef Maria Serres, Xavier Mateos, Magdalena Aguiló, Francesc Diaz, Vilejshikova Elena, Nikolai Kuleshov, Anatoly Pavlyuk, Efficient continuous-wave in-band pumped $Nd:KY(MoO_4)_2$ laser, Laser Phys. Lett. 15 (6) (2018), 065002. https://doi.org/10.1088/1612-202X/aab82f.

[9] Victor V. Atuchin, Aleksandr S. Aleksandrovsky, Bair G. Bazarov, Jibzema G. Bazarova, Olga D. Chimitova, Yuriy G. Denisenko, Tatyana A. Gavrilova, Alexander S. Krylov, Eugene A. Maximovskiy, Maxim S. Molokeev, Aleksandr S. Oreshonkov, Alexey M. Pugachev, Nikolay V. Surovtsev, Exploration of structural, vibrational and spectroscopic properties of self-activated orthorhombic double molybdate $RbEu(MoO_4)_2$ with isolated $MoO_4$ units, J. Alloy. Comp. 785 (2019) 692–697. https://doi.org/10.1016/j.jallcom.2019.01.013.

[10] Nadezhda I. Medvedeva, Anton L. Buzlukov, Vladimir V. Skachkov, Alexandra A. Savina, Vladimir A. Morozov, Yana V. Baklanova, Irina E. Animitsa, Elena G. Khaikina, Tatiana A. Denisova, Sergei F. Solodovnikov, Mechanism of sodium ion diffusion in alluaudite-type $Na_5Sc(MoO_4)_4$ from NMR experiment and ab initio calculations, J. Phys. Chem. C (2019). https://doi.org/10.1021/acs.jpcc.8b11654.

[11] Jiayue Sun, Yujing Lan, Zhiguo Xia, Haiyan Du, Sol-gel synthesis and green upconversion luminescence in $BaGd_2(MoO_4)_4:Yb^{3+},Er^{3+}$ phosphors, Opt. Mater. 33 (3) (2011) 576–581. https://doi.org/10.1016/j.optmat.2010.10.049.

[12] P.S. Dutta, A. Kumar, $Eu^{3+}$ activated molybdate and tungstate based red phosphors with charge transfer band in blue region, ECS J. Solid State Sci. Technol. 2 (2) (2013) R3153–R3167. https://doi:10.1149/2.022302jss.

[13] Chang Sung Lim, Aleksandr Aleksandrovsky, Maxim Molokeev, Aleksandr Oreshonkov, Victor Atuchin, The modulated structure and frequency upconversion properties of $CaLa_2(MoO_4)_4:Ho^{3+}/Yb^{3+}$ phosphors prepared by microwave synthesis, Phys. Chem. Chem. Phys. 17 (2015) 19278–19287. https://doi.org/10.1039/c5cp03054d.

[14] Yiru Wang, Xiaohua Liu, Lindan Jing, Pengfei Niu, Tunable white light and energy transfer of $Dy^{3+}$ and $Eu^{3+}$ doped $Y_2Mo_4O_{15}$ phosphors, Ceram. Int. 42 (2016) 13004–13010. https://doi.org/10.1016/j.ceramint.2016.05.075.

[15] Heng Wang, Ting Yang, Feng Li, Zhanglei Ning, Mengjiao Liu, Xin Lai, Daojiang Gao, Jian Bi, Energy transfer and multicolor tunable luminescence properties of $NaGd_{0.5}Tb_{0.5-x}Eu_x(MoO_4)_2$ phosphors for UV-LED, J. Electron. Mater. 47 (11) (2018) 6494–6506. https://doi.org/10.1007/s11664-018-6532-y.

[16] Olga D. Chimitova, Victor V. Atuchin, Baig G. Bazarov, Maxim S. Molokeev, Zhibzema G. Bazarova, The formation and structural parameters of new double molybdates $RbLn(MoO_4)_2$ (Ln = Pr, Nd, Sm, Eu), Proc. SPIE 8771 (2013) 877711A. https://doi.org/10.1117/12.2017816.

[17] Artem A. Abakumov, Vladimir A. Morozov, Alexander A. Tsirlin, Johan Verbeeck, Joke Hadermann, Cation ordering and flexibility of the $BO_4^{2-}$ tetrahedra in incommensurately modulated $CaEu_2(BO_4)_4$ (B = Mo, W) scheelites, Inorg. Chem. 53 (2014) 9407–9415. https://doi.org/10.1021/ic5015412.

[18] Rajagopalan Krishnan, Jagannathan Thirumalai, Venkatakrishnan Mahalingam, Srinivas Mantha, Manthramoorthy Lavanya, Synthesis, Luminescence and photometric characteristics of $Ca_{0.5}La(MoO_4)_2:Ln^{3+}$ (Ln = Eu, Tb, Dy) phosphors, Mater. Chem. Phys. 162 (2015) 41–49. https://doi.org/10.1016/j.matchemphys.2015.04.050.

[19] J.V.B. Moura, G.S. Pinheiro, J.V. Silveira, P.T.C. Freire, B.C. Viana, C. Luz-Lima, $NaCe(MoO_4)_2$ microcrystals: hydrothermal synthesis, characterization and photocatalytic performance, J. Phys. Chem. Solids 111 (2017) 258–265.

[20] L.F. Johnson, Optical maser characteristics of rare-earth ions in crystals, J. Appl. Phys. 34 (4) (1963) 897–909. https://doi.org/10.1063/1.1729557.

[21] M. Minowa, K. Itakura, S. Moriyama, W. Ootani, Measurement of the property of cooled lead molybdate as a scintillator, Nucl. Instrum. Methods Phys. Res. 320 (3) (1992) 500–503. https://doi.org/10.1016/0168-9002(92)90945-Z.

[22] S. Takano, S. Esashi, K. Mori, T. Namikata, Growth of high-quality single crystals of lead molybdate, J. Cryst. Growth 24–25 (1974) 437–440. https://doi.org/10.1016/0022-0248(74)90353-4.

[23] E. Guermen, E. Daniels, J.S. King, Crystal structure refinement of $SrMoO_4$, $SrWO_4$, $CaMoO_4$, and $BaWO_4$ by neutron diffraction, J. Chem. Phys. 55 (1971) 1093–1097. https://doi.org/10.1063/1.1676191.

[24] M. Daturi, G. Busca, M.M. Borel, A. Leklaire, P. Piaggio, Vibrational and XRD study of the system $CdWO_4$-$CdMoO_4$, J. Phys. Chem. B 101 (22) (1997) 4358–4369. https://doi.org/10.1021/jp963008x.

[25] V. Nassif, R.E. Carbonio, J.A. Alonso, Neutron diffraction study of the crystal structure of $BaMoO_4$: a suitable precursor for metalic $BaMoO_3$ perovskite, J. Solid State Chem. 146 (1) (1999) 266–270. https://doi.org/10.1006/jssc.1999.8352.

[26] V.V. Atuchin, O.D. Chimitova, T.A. Gavrilova, M.S. Molokeev, Sung-Jin Kim, N.V. Surovtsev, B.G. Bazarov, Synthesis, structural and vibrational properties of microcrystalline $RbNd(MoO_4)_2$, J. Cryst. Growth 318 (2011) 683–686. https://doi.org/10.1016/j.jcrysgro.2010.09.076.

[27] V.V. Atuchin, O.D. Chimitova, S.V. Adichtchev, J.G. Bazarov, T.A. Gavrilova, M.S. Molokeev, N.V. Surovtsev, ZhG. Bazarova, Synthesis, structural and vibrational properties of microcrystalline $RbSm(MoO_4)_2$, Mater. Lett. 106 (2013) 26–29. https://doi.org/10.1016/j.matlet.2013.04.039.

[28] Chang Sung Lim, Aleksandr S. Aleksandrovsky, Maxim S. Molokeev, Aleksandr S. Oreshonkov, Denis A. Ikonnikov, Victor V. Atuchin, Triple molybdate scheelite-type upconversion phosphor $NaCaLa(MoO_4)_3:Er^{3+}/Yb^{3+}$: structural and spectroscopic properties, Dalton Trans. 45 (2016) 15541–15551. https://doi.org/10.1039/c6dt02378a.

[29] Chang Sung Lim, Aleksandr S. Aleksandrovsky, Maxim S. Molokeev, Aleksandr S. Oreshonkov, Denis A. Ikonnikov, Victor V. Atuchin, Microwave synthesis and spectroscopic properties of ternary scheelite-type molybdate phosphors $NaSrLa(MoO_4)_3:Er^{3+},Yb^{3+}$, J. Alloy. Comp. 713 (2017) 156–163. https://doi.org/10.1016/j.jallcom.2017.04.060.

[30] R.D. Shennon, Revised effective ionic radii and systematic studies of interatomic distances in halides and chalcogenides, Acta Crystallogr. A 32 (5) (1976) 751–767. https://doi.org/10.1107/S0567739470001551.

[31] Jing Zhou, Qian Liu, Wei Feng, Yun Sun, Fuyou Li, Upconversion luminescent materials: advances and applications, Chem. Rev. 115 (1) (2015) 395–465. https://doi.org/10.1021/cr400478f.

[32] Chang Sung Lim, Aleksandr Aleksandrovsly, Maxim Molokeev, Aleksandr Oreshonkov, Victor Atuchin, Microwave sol-gel synthesis and upconversion photoluminescence properties of $CaGd_2(WO_4)_4:Er^{3+}/Yb^{3+}$ phosphors, J. Solid State Chem. 228 (2015) 160–166. https://doi.org/10.1016/j.jssc.2015.04.032.

[33] Fangrui Cheng, Zhiguo Xia, Xiping Jing, Ziyuan Wang, Li/Ag ratio dependent structure and upconversion photoluminescence of $Li_xAg_{1-x}Yb_{0.99}(MoO_4)_2$:$0.01Er^{3+}$ phosphors, Phys. Chem. Chem. Phys. 17 (2015) 3689–3696. https://doi.org/10.1039/C4CP03950E.

[34] Chang Sung Lim, Victor Atuchin, Aleksandr Aleksandrovsky, Maxim Molokeev, Aleksandr Oreshonkov, Microwave sol-gel synthesis of $CaGd_2(MoO_4)_4:Er^{3+}/Yb^{3+}$ phosphors and their upconversion photoluminescence properties, J. Am. Ceram. Soc. 98 (10) (2015) 3223–3230. https://doi.org/10.1111/jace.13739.

[35] Ming-Jun Song, Yan Zhang, Na-Na Zhang, Lin-Tong Wang, Qin-Guo Meng, Upconversion properties of $Er^{3+}/Yb^{3+}$ co-doped $Li_3Ba_2Gd_3(MoO_4)_8$ phosphors, Chin, J. Struct. Chem. 37 (2) (2018) 210–218. https://doi.org/10.14102/j.cnki.0254-5861.2011-1753.

[36] Kirill I. Rybakov, Eugene A. Olevsky, Ekaterina V. Krikun, Microwave suntering: fundamentals and modeling, J. Am. Ceram. Soc. 96 (4) (2013) 1003–1020. https://doi.org/10.1111/jace.12278.

[37] Helen J. Kitchen, Simon R. Vallance, Jennifer L. Kennedy, Nuria Tapia-Ruiz, Lucia Carassiti, Andrew Harrison, A. Gavin Whittaker, Timothy D. Drysdale, Samuel W. Kingman, Duncan H. Gregory, Modern microwave methods in solid-state inorganic materials chemistry: from fundamentals to manufacuring, Chem. Rev. 114 (2014) 1170–1206. https://doi.org/10.1021/cr4002353.

[38] Jeong Ho Ryu, Sang-Mo Koo, Dong Suk Chang, Jong-Won Yoon, Chang Sung Lim, Kwang Bo Shim, Microwave-assisted synthesis of $PbWO_4$ nano-powders via a citrate complex precursor and its photoluminescence, Ceram. Int. 32 (6) (2006) 647–652. https://doi.org/10.1016/j.ceramint.2005.04.025.

[39] Chang Sung Lim, Upconversion photoluminescence properties of $SrY_2(MoO_4)_4:Er^{3+}/Yb^{3+}$ phosphors synthesized by a cyclic microwave-modified sol-gel method, Infrared Phys. Technol. 67 (2014) 371–376. https://doi.org/10.1016/j.infrared.2014.08.018.

[40] V.V. Atuchin, V.G. Grossman, S.V. Adichtchev, N.V. Surovtsev, T.A. Gavrilova, B.G. Bazarov, Structural and vibrational properties of microcrystalline $TlM(MoO_4)_2$ (M = Nd, Pr) molybdates, Opt. Mater. 34 (2012) 812–816. https://doi.org/10.1016/j.optmat.2011.11.016.

[41] Tao Wu, Yunfei Liu, Yinong Lu, Ling Wei, Hong Gao, Hu Chen, Morphology-controlled synthesis, characterization, and luminescence properties of $KEu(MoO_4)_2$ microcrystals, CrystEngComm 15 (2013) 2761–2768. https://doi.org/10.1039/C3CE27073D.

[42] V.V. Atuchin, A.S. Aleksandrovsky, O.D. Chimitova, T.A. Gavrilova, A.S. Krylov,

M.S. Molokeev, A.S. Oreshonkov, B.G. Bazarov, J.G. Bazarova, Synthesis and spectroscopic properties of monoclinic $\alpha$-$Eu_2(MoO_4)_3$, J. Phys. Chem. C 118 (28) (2014) 15404–15411. https://doi.org/10.1021/jp5040739.

[43] Bruker AXS TOPAS V4, General Profile and Structure Analysis Software for Powder Diffraction Data. – User's Manual, Bruker AXS, Karlsruhe, Germany, 2008.

[44] C. Lugli, L. Medici, D. Saccardo, Natural wulfenite: structural refinement by single-crystal X-ray diffraction, Neues Jahrb. Mineral. Monatshefte (6) (1999) 281–288.

[45] T.I. Bylichki, L.I. Soleva, E.A. Pobedims, N.A. Poraikos, N.V. Belov, Crystal structures of Ba molybdate and Ba tungstate, soviet physics crystallography, USSR 15 (1) (1970) 130.

[46] I.C. Nogueira, L.S. Cavalcante, P.F.S. Pereira, M.M. De Jesus, J.M. Rivas Mercury, N.C. Batista, M. Siu Li, E. Longo, Rietveld refinement, morphology and optical properties of $(Ba_{1-x}Sr_x)$ $MoO_4$ crystals, J. Appl. Crystallogr. 46 (5) (2013) 1434–1446. https://doi.org/10.1107/S0021889813020335.

[47] P. Gall, P. Gougeon, The scheelite-type europium molybdate $Eu_{0.96}MoO_4$, Acta Crystallogr. 62 (5) (2006) i120–i121. https://doi.org/10.1107/S1600536806012803.

[48] G. Raymond, Teller, Refinement of some $Na_{0.5-x}M'_{0.5+x/32x/3}MoO_4$, M' = Bi, Ce, La, scheelite structures with powder neutron and X-ray diffraction data, Acta Crystallogr. C 48 (12) (1992) 2101–2104. https://doi.org/10.1107/S0108270192001434.

[49] R.M. Hazen, L.W. Finger, J.W. Mariathasan, High-pressure crystal chemistry of scheelite-type tungstates and molybdates, J. Phys. Chem. Solids 46 (2) (1985) 253–263. https://doi.org/10.1016/0022-3697(85)90039-3.

[50] Chang Sung Lim, Microwave sol-gel derived $NaCaGd(MoO_4)_3$:$Er^{3+}$/$Yb^{3+}$ phosphors and their upconversion photoluminescence properties, Infrared Phys. Technol. 76 (2016) 353–359. https://doi.org/10.1016/j.infrared.2016.02.012.

[51] J. Hanuza, M. Maczka, Vibrational properties of the double molybdates $MX(MoO_4)_2$ family (M = Li,Na,K,Cs; X = Bi,Cr) Part I. Structure and infrared and Raman spectra in the polycrystalline state, Vib. Spectrosc. 7 (1) (1994) 85–96. https://doi.org/10.1016/0924-2031(94)85044-5.

[52] K. Nakamoto, Infrared and Raman Spectra of Inorganic and Coordination Compounds, sixth ed., Wiley, New York etc., 2009.

[53] D.A. Ikonnikov, V.N. Voronov, M.S. Molokeev, A.S. Aleksandrovsky, Upconversion luminescence of $CsScF_4$ crystals doped with erbium and ytterbium, Opt. Mater. 60 (2016) 584–589. https://doi.org/10.1016/j.optmat.2016.09.016.